Sensitivity Analysis of Full-waveform LiDAR Data for Material Classification

Omar Aldohami and Hristo Vassilev
Chair of Building Informatics and Geoinformation Systems and Geodetic Institute, RWTH Aachen University, Mies-van-der-Rohe-Str. 1, 52074 Aachen, Germany
E-mail(s): omar.aldohami@rwth-aachen.de, hristo.vassilev@gia.rwth-aachen.de

Abstract: Full-waveform (FWF) LiDAR can provide additional features which can be helpful to distinguish between different construction materials. However, due to its high volume FWF information is often discarded and not used for downstream analysis, such as material classification. This contribution investigates waveform processing, such as Gaussian decomposition, and modelling to extract important radiometric features from terrestrial laser scanning. In addition, geometric information is extracted by analysing point cloud neighbourhoods. The resulting combination of features is evaluated by means of sensitivity analysis to obtain their corresponding relevance to material classification. Specifically, the assessment is performed leveraging machine learning algorithms, such as support vector machines, and monitoring the influence of the model's performance depending on the combinatoric inclusion of the proposed individual features. To support the analysis, furthermore a rich dataset is presented, consisting of point clouds, waveform and image data of various urban and infrastructure scenes. Thereby the aim of the classification problem is to semantically segment the point clouds according to common materials such as concrete surfaces, vegetation or brick. This effort serves the goal of improving the automatic digitization of construction assets through the use of advanced remote sensing techniques.

Keywords: Digital Twin, Full-waveform, Laser scanning, Machine learning, Scan-to-BIM

Erschienen in Tagungsband 35. Forum Bauinformatik 2024, Hamburg, Deutschland, DOI: 10.15480/882.13519

1 Introduction

Over the last years, the demand for adopting modern data acquisition techniques, such as 3D laser scanning, for accurate Building Information Models (BIM) of existing buildings has increased in popularity. Such data include high resolution and high accuracy point cloud models which serve the purpose of downstream applications for models made using scan-to-BIM, which can range from as-built documentation, project renovations and additions, or facility management. Models made with scan-to-BIM are also very useful for comparing against as-planned models. A case study discussed the practical integration of 3D laser scanning with BIM in construction projects and demonstrated the significant impact of these technologies on improving project outcomes by enhancing as-built documentation and project information management [1].

With the introduction of full-waveform, FWF, LiDAR systems as an active remote sensing technique, emerged new possibilities for retrieving additional morphological features which can be used to enhance the automatic classification of urban areas. Typically, commercial LiDAR systems measure the first and last signal pulse, and some are capable of recording up to six echoes for each emitted pulse [2]. Due to the 3D structure of natural and artificial objects, the shape of the received signal can be extremely complex and these traditional discrete return systems can only provide the coordinates of the scattering objects. Conversely, full-waveform data capture the sequential 1D profiles of the landscape, where the laser beam, penetrating a cone-shaped volume due to diffraction, registers each object within this volume as distinct echoes in the waveform [3]. Full waveform return systems can therefore enhance user control over the interpretation of physical measurements and offer additional details about the reflectance of back-scattered objects. By combining full waveform feature extraction with machine learning, The aim is to assess the relevance of the additional waveform features in the specific use case of using TLS for "As-Is" / "As-Built" scan-to-BIM.

2 Research Background

2.1 Physical Operating Principle of FWF Systems

LiDAR is an active remote sensing technology that emits its own energy, unlike passive systems that rely on ambient light. LiDAR systems emit light signals toward the Earth's surface, which interact with objects like buildings and trees. The reflected light returns to the sensor, where it is detected and recorded. The time interval between the emission and return of the light signal, known as the two-way travel time, is used to calculate the distance traveled by the light signal, converting it into Cartesian coordinates. FWF LiDAR systems capture multiple reflections, or "returns," from a single laser signal, which are all recorded by the sensor. The returning light energy generates a waveform, representing the energy distribution detected by the sensor. Peaks in the waveform correspond to different objects encountered by the laser signal, such as branches or buildings. Analyzing these waveforms allows for extracting detailed morphological features, enhancing the classification and mapping of various objects within the scanned environment.

2.2 Development of FWF LiDAR

The development and application of full-waveform (FWF) LiDAR systems have significantly ad-vanced remote sensing. The first operational FWF LiDAR, the Laser Vegetation Imaging Sensor (LVIS), was developed by NASA in 1999. LVIS showcased the utility of recording entire waveforms for detailed vegetation analysis, capturing complex structural information of vegetation canopies [4]. The first commercial FWF LiDAR system was introduced in 2004, and today, companies like Riegl, Optech, Leica, and propose such an extension to their multiple pulse devices [5]. FWF LiDAR technology shows promise across various fields, for instance in forestry and environmental monitoring where it can facilitate precise tree species classification by capturing detailed waveform characteristics, improving accuracy in complex forest environments [6]. In coastal and underwater surveying, such as in the German Wadden Sea National Park, FWF LiDAR enhanced seabed map-ping and habitat structure analysis, highlighting its utility in environmental planning and conservation efforts in aquatic environments [7].

While FWF data have been used mainly for a large variety of land-cover mapping in forestry and vegetated areas using airborne laser scanning devices, theoretical assessment of the potential of such data has been barely tackled [8]. This is due to several factors: the complexity of waveform processing, the much larger data volume compared to multi-echo data, and the lack of standard formats and software solutions. Furthermore, FWF terrestrial laser scanning systems often exhibit more non-linearity in the scale characteristics of the system's response than observed in the FWF data acquired by airborne LiDAR systems. This is often due to the high dynamic range of the TLS targets (due to large range envelope) [9].

2.3 FWF Processing

Waveform processing in FWF LiDAR involves signal processing methods to decompose complex waveforms into identifiable echoes and model them using suitable mathematical functions. This process effectively characterizes different targets encountered by the laser pulse, extracting meaningful waveform-derived features.

2.3.1 Waveform Decomposition and Modelling

Initially, the goal is to maximize the detection rate of relevant peaks within the waveforms. This is done by waveform decomposition through which these complex waveforms are analyzed to identify the echo positions. An echo is generated when the laser signal reflects off an object and returns to the LiDAR sensor. The position of each echo within the waveform is critical as it relates directly to the physical location and characteristics of the object in the environment. Peak detection algorithms can help achieve this by identifying points in the data where the signal reaches a local maximum that is significant against the background noise. After detecting peaks, initial estimation of component numbers and values, is followed by parameter optimization to refine these estimates. Effective wave-form processing relies heavily on precise initial parameter estimation to prevent errors in echo characterization. Established techniques for optimization in the literature include the Expectation-Maximization algorithm, suitable for Maximum Likelihood estimates, and the Levenberg-Marquardt algorithm for non-linear least squares approaches [10]. Parametric modelling of echoes reveals detailed information about the surface or object from which the laser light was reflected. The shape of an echo depends on attributes like material reflectivity, object geometry, and laser beam angle. Gaussian functions, Lognormal, or a sum of generalized Gaussian (GG) curves often represent these echoes. Wagner et al. (2006) showed that more than 98% of observed waveforms with the Riegl system could be fitted with a sum of Gaussian functions. Asymmetric echoes, frequently observed in certain waveforms, necessitate adaptable parametric functions, capturing nuances such as skewness and scale [10].

2.3.2 Potential of FWF Features

FWF features capture detailed physical characteristics of targets, distinguishing different surfaces in urban environments. For instance, echo width and amplitude help identify vegetative or soft surfaces versus hard surfaces like roads. Reflectance variations can discern materials, which helps distinguish a building's concrete façade from glass windows, for example as shown in Figures 1 and 2 below.

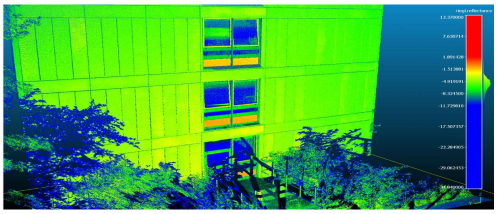

Figure 1: Reflectance variations

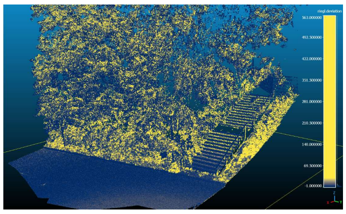

Figure 2: Deviation (echo width) variations

3 Methods

3.1 Study Area and Dataset

The following section describes the processing chain used in this study. Initially, the process begins with scanning the urban environment in the city of Aachen, Germany, focusing on areas which include both natural and man-made structures. Target selection was based on locations with various building facades made from different construction materials. RWTH Institute for Physical Chemistry and RWTH Chemistry Institute buildings were selected as the study areas. The selected classes of targets were to be located at different distances (ranges) from the scanner. Data acquisition targeted five classes of interest: Concrete, Bricks, Artificial ground, Natural ground, and Vegetation. The data was collected using the Riegl VZ-400 FWF Terrestrial Laser Scanner [11], for which dataset illustrations are shown in Figure 3.

Figure 3: Illustrations of dataset

3.2 FWF Processing

The following section describes the processing chain, depicted in Figure 4. Initially, the raw data is captured and exported in two formats: TLS LiDAR Waveforms (.wfm) and 3D point clouds (.rdbx). By combining the data found in those two formats, the point cloud generated by manufacturer's proprietary algorithms is merged with the raw full-waveform signal used in the process. The linking between the extracted point cloud and the corresponding location in the waveform data is facilitated through a timestamp. The waveform data consists of regions of interest (ROI), which are extracted from the entirety of the received signal during the on-board processing of the TLS. Although the ROI may initially vary in length, it was constrained to 32 values per point for consistency. Waveform processing involves the detection and modeling of peaks within the digitized echo signals, representing potential tar-gets or features. The findpeaks function from the SciPy library identifies local maxima based on amplitude and other properties such as prominence and width. Prominence measures how much a peak stands out from the surrounding baseline, calculated as the vertical distance between the peak and the lowest con-tour around it that does not contain any higher peak. Peak width at a relative height is also calculated to ensure the peaks represent true signal characteristics. Once peaks are identified, a single Gaussian modelling is used in artificial classes which often exhibit single peak.

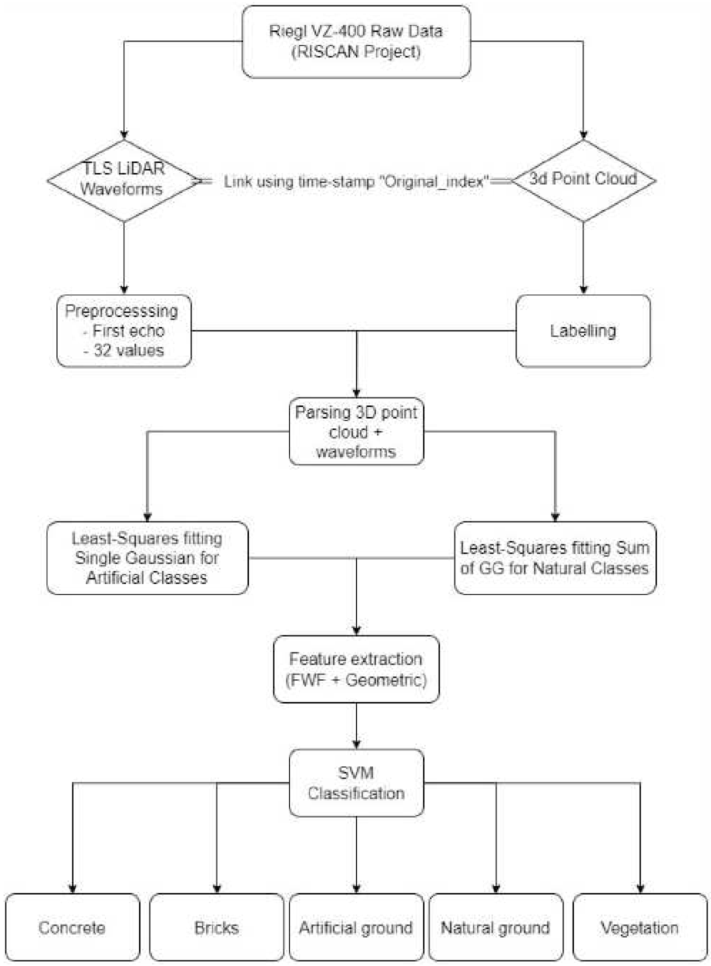

Figure 4: Flowchart for the processing chain.

The *curvefit* function in Scipy fits the data points of each detected peak by optimizing the parame-ters to minimize the difference between the fitted curve and the actual data points. The Gaussian fitting optimization utilizes the Levenberg-Marquardt algorithm which adeptly balances gradient descent and Gauss-Newton methods, optimizing parameter estimation for non-linear least squares problems. The algorithm starts with initial parameter guesses based on detected peak properties and enforces parameter bounds to ensure realistic solutions by handling up to 10,000 function evaluations (iterations). To assess the accuracy of the fit, Residuals, calculated as the difference be-tween observed data points and model-predicted values are measured with metrics such as R-squared and Root Mean Square Error (RMSE) to validate the model's effectiveness. An R-squared value of 0.9676 achieved indicates that approximately 96.76% of the variance in the dependent variable is explained by the model, suggesting a strong correlation and effective model performance. In complex environments like natural ground and vegetation, waveforms often exhibit multiple peaks due to overlapping features or mixed material responses. A sum of generalized Gaussians model is then used to effectively fit the multiple peaks variations. This model captures diverse peak shapes which are noticed in natural classes. Fitting of waveforms is illustrated in Figure 5 below.

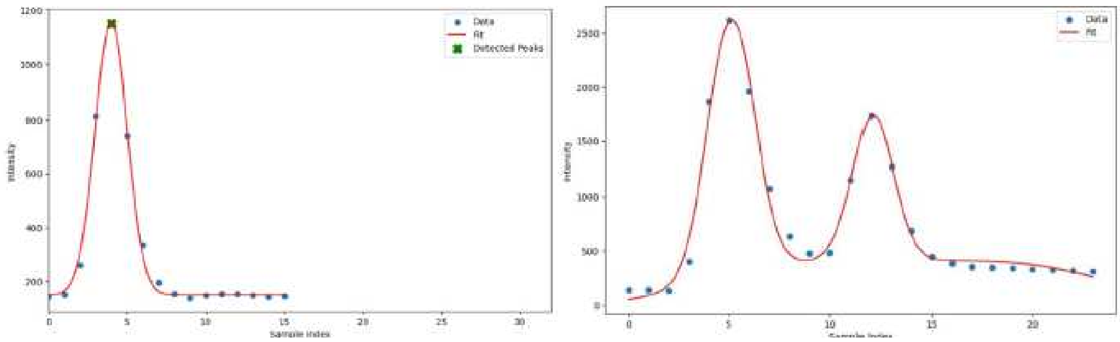

Figure 5: Left graph shows single Gaussian fitting for a 'Bricks' class waveform; right graph depicts a sum of generalized Gaussian fits for a 'Vegetation' sample.

3.3 Features of Interest

Several critical FWF features are extracted to characterize the waveform's profile, such as amplitude and mean, which indicate the peak intensity and central location of each peak, respectively, providing essential information on the strength and position of reflections. Sigma (σ), or the standard deviation of the Gaussian fit, illustrates the spread of the waveform around the mean, indicative of surface irregularities or scattering effects. Echo Width at Half Maximum (EWHM) quantifies the width at half-maximum intensity. The Peak Area under the Gaussian curve represents the total power of the reflected signal, correlating with the physical attributes of the reflecting surface. Flatness and Echo Asymmetry describe the peakedness and symmetry of the waveform, respectively, offering insights into the directional properties and uniformity of the reflecting surfaces. Statistical measures like Skewness and Kurtosis provide further description of the waveform's shape, assessing the asymmetry and tailedness which help distinguish material types based on reflective properties. Additionally, Peak Count and Average Inter-Peak Distance gauge the complexity of the waveform, which can be helpful to distinguish natural classes with multiple peaks from artificial ones. In addition, geometric local features were computed in Cloud Compare software. Roughness measures surface texture variation. Mean and Gaussian curvatures help distinguish surface shapes, such as flat, con-vex, and concave structures, useful for identifying man-made versus natural formations. Eigenvalues from principal component analysis yield shape descriptors like omnivariance, eigenentropy, and anisotropy, which indicate linear, planar, or volumetric features. Surface and volume density metrics quantify point distribution. Verticality assesses point alignment relative to the vertical axis, differentiating vertical structures like buildings from the ground plane. Figure 5 shows some derived features distinguishing between different classes. Feature selection strategy in this paper is based on ANOVA F-Score and SVM Coefficients for identifying the most informative features. ANOVA F-Score evaluates the impact of features based on statistical significance across groups, while SVM Coefficients reflect feature importance based on their role in the model's decision boundary.

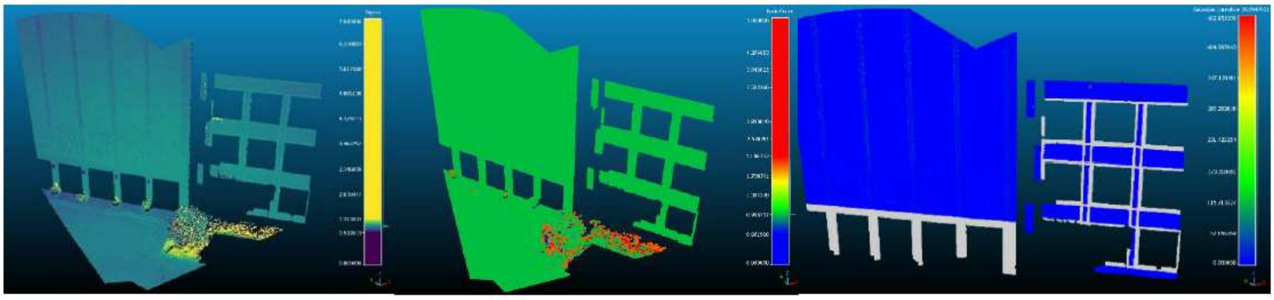

Figure 6: Derived features such as σ, peak count, and Gaussian curvature.

4 Results and Discussion

The model was trained on a dataset consisting of building facades with various materials and tested on a third building facade. Figure 6 illustrates the global feature ranking by averaging their importance across ANOVA F-Score and SVM Coefficient-based Feature Importance methods, with FWF features highlighted in bold. Additionally, a one-vs-one SVM approach with an RBF kernel was implemented to differentiate between natural and artificial classes. Using the FWF features, the recall and F1-score for natural classes increased from 0.75 and 0.86 to 0.86 and 0.92, respectively.

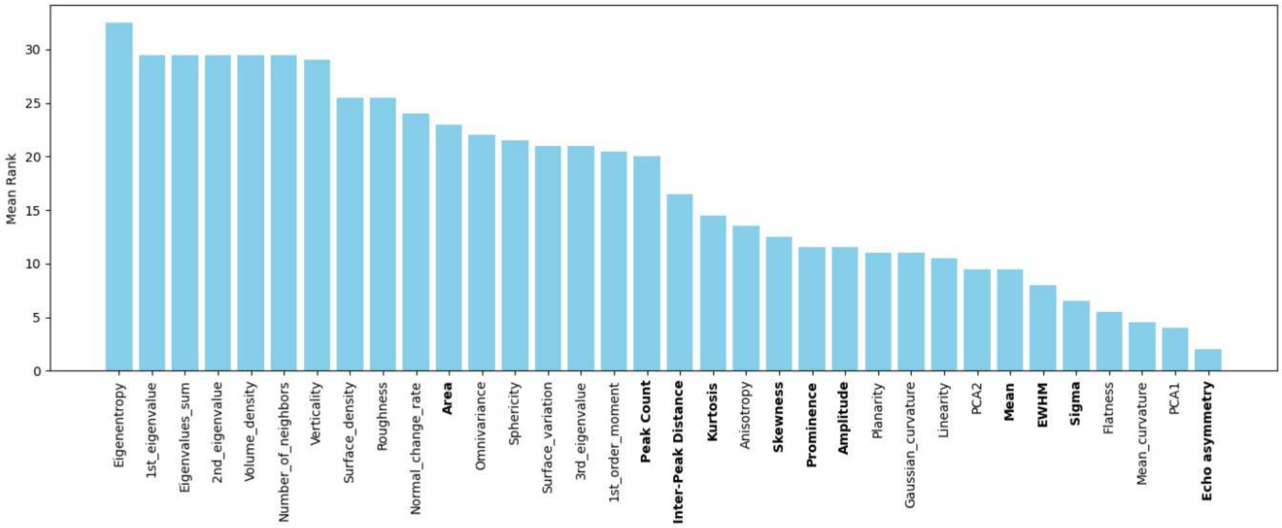

Figure 7: Global ranking using the two techniques. The mean rank is plotted for each feature.

5 Conclusion

This paper examined the classification of 3D point clouds in urban areas using terrestrial scanner full-waveform (FWF) data. The goal was to create an objective workflow to evaluate the impact of FWF features on classification. A supervised SVM classifier was used with a 34-component feature vector, including 11 FWF features. It was found that features like area, peak count, and average inter-peak distance are highly discriminative, while echo asymmetry and mean are less so. Future work could involve adding Riegl's proprietary features (reflectance, amplitude, deviation) and features from radiometric calibration (cross-section, back-scatter coefficient) to improve classification. Additionally, data mining techniques could reduce feature redundancy before selection.

References

[1] F. Sadeghineko, K. Lawani, and M. Tong, “Practicalities of incorporating 3d laser scanning with bim in live construction projects: A case study”, *Buildings*, vol. 14, no. 6, p. 1651, 2024.

[2] A. Chauve, S. Durrieu, F. Bretar, M. Pierrot-Deseilligny, and W. Puech, “Processing full-waveform lidar data to extract forest parameters and digital terrain model: Validation in an alpine coniferous forest”, *International Journal of Remote Sensing*, vol. 30, no. 19, pp. 5211–5237, 2009.

[3] C. Mallet, F. Bretar, M. Roux, U. Soergel, and C. Heipke, “Relevance assessment of full-waveform lidar data for urban area classification”, *ISPRS Journal of Photogrammetry and Remote Sensing*, vol. 66, no. 6, Supplement, S71–S84, 2011.

[4] J. B. Blair, D. L. Rabine, and M. A. Hofton, “The laser vegetation imaging sensor: A medium-altitude, digitisation-only, airborne laser altimeter for mapping vegetation and topography”, *ISPRS Journal of Photogrammetry and Remote Sensing*, vol. 54, pp. 115–122, 1999.

[5] F. Bretar, A. Chauve, C. Mallet, and B. Jutzi, “Managing full waveform lidar data: A challenging task for the forthcoming years”, in *ISPRS Congress Proceedings*, ser. Part B1, ISPRS, vol. XXXVII, 2008, pp. 69–74.

[6] G. Zhao, A. Sanchez-Azofeifa, K. Laakso, C. Sun, and L. Fei, “Hyperspectral and full-waveform lidar improve mapping of tropical dry forest’s successional stages”, *Remote Sensing*, vol. 13, no. 19, p. 3830, 2021.

[7] D. Mader, K. Richter, P. Westfeld, J.-G. Nistad, and H.-G. Maas, “Analysis of the potential of full-waveform stacking techniques applied to coastal airborne lidar bathymetry data of the german wadden sea national park”, *International Hydrographic Review*, vol. 29, no. 2, pp. 46–64, 2023.

[8] N. Chehata, L. Guo, and C. Mallet, “Airborne lidar feature selection for urban classification using random forests”, in *International Archives of Photogrammetry, Remote Sensing and Spatial Information Sciences*, ser. Part 3/W8, vol. 38, 2009, pp. 207–212.

[9] M. Pashaei, M. J. Starek, C. L. Glennie, and J. Berryhill, “Classification of terrestrial lidar data directly from digitized echo waveforms”, *IEEE Transactions on Geoscience and Remote Sensing*, vol. 61, 2023.

[10] M. Wagner, H. Ullrich, S. Ducic, M. Melzer, and N. Studnicka, “Gaussian decomposition and calibration of a novel small-footprint full-waveform digitising airborne laser scanner”, *ISPRS Journal of Photogrammetry and Remote Sensing*, 2006.

[11] RIEGL Laser Measurement Systems GmbH, *Data sheet: Vz-400 terrestrial laser scanner*, 2017. [Online]. Available: http://www.riegl.com/uploads/tx_pxriegldownloads/10_DataSheet_VZ-400_2017-06-14.pdf.